remote sensing

MDPI

Article

Estimation of $PM_{2.5}$ and PM_{10} Mass Concentrations in Beijing Using Gaofen-1 Data at 100 m Resolution

Shuhui Wu [1,2], Yuxin Sun [1], Rui Bai [1], Xingxing Jiang [1], Chunlin Jin [1] and Yong Xue [1,3,*]

[1] School of Environment and Spatial Informatics, China University of Mining and Technology, Xuzhou 221116, China; wush@cumt.edu.cn (S.W.); sunyx@cumt.edu.cn (Y.S.); br_123up@163.com (R.B.); xxj@cumt.edu.cn (X.J.); chunlinj@cumt.edu.cn (C.J.)

[2] Artificial Intelligence Research Institute, China University of Mining and Technology, Xuzhou 221116, China

[3] School of Computing and Mathematics, College of Science and Engineering, University of Derby, Kedleston Road, Derby DE22 1GB, UK

* Correspondence: y.xue@derby.ac.uk; Tel.: +86-139-1053-5998

Abstract: Due to the advantage of high spatial coverage, using satellite-retrieved aerosol optical depth (AOD) data to estimate $PM_{2.5}$ and PM_{10} mass concentrations is a current research priority. Statistical models are the common method of PM estimation currently, which do not require the knowledge of complex chemical and physical interactions. However, the statistical models rely on station data, which results in less accurate PM estimation concentrations in areas where station data are missing. Hence, a new hybrid model, with low dependency on on-site data, was proposed for $PM_{2.5}$ and PM_{10} mass concentration estimation. The Gaofen-1 satellite and MODIS data were employed to estimate $PM_{2.5}$ and PM_{10} concentrations with 100 m spatial resolution in Beijing, China. Then, the estimated $PM_{2.5/10}$ mass concentration data in 2020 were employed to conduct a spatio-temporal analysis for the investigation of the particulate matter characteristic in Beijing. The estimation result of $PM_{2.5}$ was validated by the ground stations with R^2 ranging from 0.91 to 0.98 and the root mean square error (RMSE) ranging from 4.51 $\mu g/m^3$ to 17.04 $\mu g/m^3$, and that for PM_{10} was validated by the ground stations with R^2 ranging from 0.85 to 0.98 and the RMSE ranging from 6.98 $\mu g/m^3$ to 29.00 $\mu g/m^3$. The results showed that the hybrid model has a good performance in $PM_{2.5/10}$ estimation and can improve the coverage of the results without sacrificing the effectiveness of the model, providing more detailed spatial information for urban-scale studies.

Keywords: AOD; Gaofen-1; $PM_{2.5}$; PM_{10}; remote sensing; urban air pollution

check for updates

Citation: Wu, S.; Sun, Y.; Bai, R.; Jiang, X.; Jin, C.; Xue, Y. Estimation of $PM_{2.5}$ and PM_{10} Mass Concentrations in Beijing Using Gaofen-1 Data at 100 m Resolution. *Remote Sens.* **2024**, *16*, 604. https://doi.org/10.3390/rs16040604

Academic Editor: Alexander Marshak

Received: 17 December 2023
Revised: 28 January 2024
Accepted: 30 January 2024
Published: 6 February 2024

1. Introduction

Numerous health-related studies have shown that exposure to $PM_{2.5}$ and PM_{10} increases morbidity and mortality from a number of diseases, most of which are respiratory and cardiovascular diseases [1–5]. There are even adverse effects on the weights and lengths of newborns [6]. In 2010 and 2014, severe $PM_{2.5}$ pollution caused over 1.2 million and 1.6 million deaths, respectively [7,8]. As the economy and cities grow in China, PM has become one of the most serious pollutants of air pollution and a widespread concern [9,10].

The existing studies using ground-based stations for air quality assessment can provide high-precision results, but the ground-based monitoring methods inevitably face some problems, such as limited spatial coverage and uneven station distribution [11–13]. To overcome the above shortcomings, satellite remote sensing techniques are increasingly being studied for estimating $PM_{2.5/10}$ concentrations due to their high resolution and wide spatial and temporal coverage [14–17]. The linear regression of aerosol optical depth AOD-$PM_{2.5}$ is employed to represent the correlation in many previous studies [18,19]. However, several studies have demonstrated that there is a non-linear relationship between AOD and $PM_{2.5}$ [20,21]. In addition to this, there are several studies based on other methods such as chemical transport simulation and physical correction for PM estimation [22–26]. Among these models, statistical models are the most popular in academia, which include mainly empirical statistical models, such as multiple linear regression [21,27], the mixed effects model [28,29], geographically weighted regression models (GWR) and their derivative models [30–33], the generalized additivity model (GAM) [34–37], and machine learning, such as random forest [38–40], support vector regression [41,42], and neural network models [43–45]. Specifically, the GWR model is a spatial statistical technique used to explore and model spatially varying relationships, which recognizes the variability in connections between variables across geographical locations, enabling focused modeling and analysis. Song et al. applied a specific satellite-based GWR model to obtain $PM_{2.5}$ over the Pearl River Delta region in China, and developed more accurate large-scale $PM_{2.5}$ monitoring [46]. The improved geographically and temporally weighted regression (IGTWR) model is developed based on the traditional GWR model, which incorporates both spatial and temporal dimensions to improve the accuracy of predictions. He and Huang employed the IGTWR model for estimating high-resolution $PM_{2.5}$ over the Beijing–Tianjin–Hebei region of China [47]. By combining temporal and spatial weights, the IGTWR model can consider the geographical and temporal variations of $PM_{2.5}$ concentrations. This approach recognizes the temporal fluctuations in air quality and provides a more comprehensive and accurate representation of the factors influencing $PM_{2.5}$ levels over time.

Urban structures are closely correlated with air pollution [48]. To further understand the mechanisms of the models, validate modeling results, and improve modeling capabilities, the particulate matter estimation for urban agglomerations requires high spatial and temporal resolution observations [49]. The Gaofen-1 (GF-1) satellite is a high-resolution Earth observation satellite developed by China. GF-1, launched on 26 April 2013, is part of China's high-resolution Earth observation system (Hi-ResEOS), and also represents a significant milestone in China for enhancing satellite remote sensing capabilities. It can improve its role in Earth observation with several key features and capabilities it possesses. With advanced optical instruments, it can offer more detailed observations of Earth's surface features. Additionally, its wide swath coverage can efficiently monitor large areas in a single pass and contribute to comprehensive Earth monitoring. Moreover, GF-1 supports versatile imaging modes, including panchromatic and multispectral, enabling a range of applications in environmental monitoring, pollution assessment, and various applications related to Earth observation. These features collectively make GF-1 a valuable asset for diverse remote sensing endeavors. Several studies have been conducted to retrieve AOD at 160 m spatial resolution and calculate $PM_{2.5}$ using the Gaofen-1 satellite [50,51]. Furthermore, the AOD data from the moderate resolution imaging spectroradiometer (MODIS) satellite have a high temporal resolution, global coverage, diverse spectral bands, specialized algorithms, rigorous validation, and long-term record advantages. In our previous study, GF-1 wide field-of-view (WFV) and MODIS data were applied to retrieve AODs at a spatial resolution of 100 m [52]. Then, these AODs were employed to estimate $PM_{2.5}$ and PM_{10} concentrations at this resolution using an IGTWR model incorporating a proportional relationship formula. The spatial pattern and accuracy of GF $PM_{2.5/10}$ estimates were assessed using tenfold cross-validation, leave-one-out validation, and validation based on in situ monitoring data. Finally, the limitations of GF $PM_{2.5/10}$ in this study are discussed, and future work is proposed to address the limitations in resolution and accuracy.

2. Study Area and Data

2.1. Study Region

The primary area of focus in this study is Beijing, centered at longitude 116°20′ East and latitude 39°56′ North, a world-famous ancient capital and modern international city. As illustrated in Figure 1, Beijing has 23 types of land use and 24 air quality stations. Due to industrialization and urbanization in recent years, air pollution, especially $PM_{2.5}$ and PM_{10}, has become a serious and urgent issue for Beijing [11,53,54].

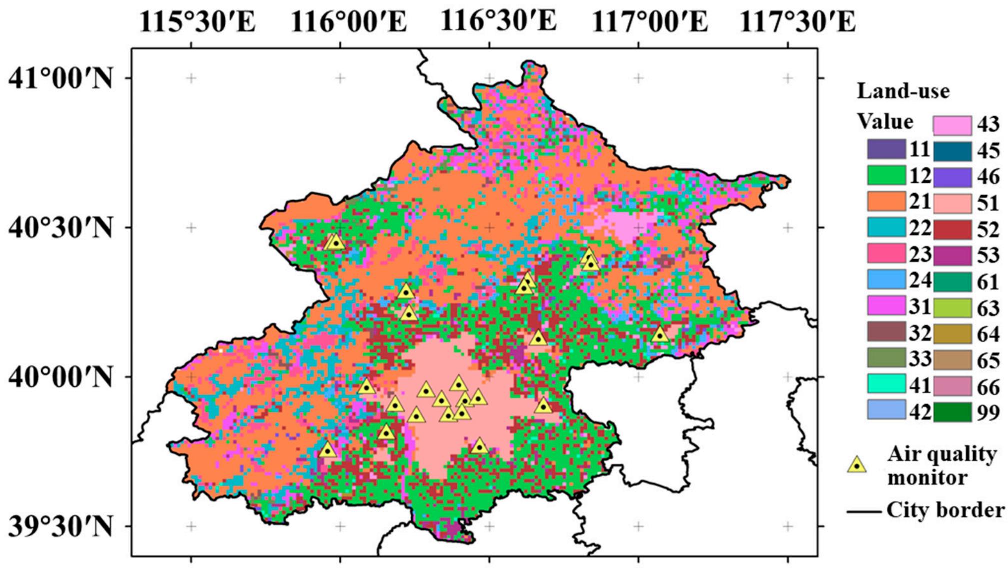

Figure 1. Study areas with the land types and locations of the air quality monitoring stations. Please refer to the Table 1 for the detailed information of land-use types.

Table 1. The land-use types in China [55].

Number	Designation	Number	Designation	Number	Designation
11	Paddy field	41	Channel	61	Sand
12	Dry land	42	Lake	62	Gobi
21	Woodland	43	Reservoir pond	63	Saline alkali soil
22	Shrub wood	44	Permanent glacier and snow	64	Swamp land
23	Sparse woodland	45	Tidal flat	65	Bare land
24	Other woodlands	46	Beach land	66	Bare rock texture
31	High-coverage grassland	51	Urban land use	67	Other
32	Medium-coverage grassland	52	Rural settlements	99	Undefined
33	Low-coverage grassland	53	Other construction land		

2.2. $PM_{2.5/10}$ Measurement Data

The $PM_{2.5/10}$ ground-based measurement data employed in the present paper are collected from the Chinese National Real-Time Air Quality Release Platform (https://air.cnemc.cn:18007/, accessed on 2 December 2023). Figure 1 shows the geographical locations of the national air quality monitoring stations within the Beijing region in 2020. The monitoring stations measure air pollutant parameters including $PM_{2.5}$, PM_{10}, and ozone. In this study, $PM_{2.5}/PM_{10}$ at 10:00 and 14:00 are adopted to correspond to the AOD data. In the section on results validation, monitoring data from 40 stations in and around the Beijing city area were used.

2.3. AOD Data

GF-1 combines high resolution with large bandwidth, and accommodates multiple spatial resolutions, multiple spectral resolutions, and integrated multi-source remote sensing data requirements. It has 16 m spatial resolution and four days' temporal resolution [56]. MODIS is a medium-resolution imaging spectrometer that carries two satellites, Terra and Aqua. It is a crucial instrument in the U.S. Earth Observing System (EOS) program and is primarily used to observe global biological and physical processes. Numerous research fields already make extensive use of the MODIS sensors on Terra and Aqua. They can offer up to two observations of visible light each day. In order to further improve the spatial resolution of the AOD data and to enhance the ability to study air pollution in small areas, Bai et al. combined two sets of satellite data to obtain a high-resolution AOD [52]. First, they collected 52 high-coverage images from the GF-1 wide field-of-view (WFV) cameras within the study area in 2020, along with corresponding MODIS data captured during the same period. The 1 km resolution 1B level data (MOD/MYD02) from MODIS were downscaled with the help of GF-1 WFV data using the mutual information (MI) algorithm [52]. In this process, MI quantifies the statistical dependence between two variables by measuring the amount of information one variable provides about the other, and computes the entropy of each variable and their joint entropy for capturing the uncertainty and information shared between them [57,58]. Then, the downscaled TERRA and AQUA satellite data are used to retrieve AOD by the synergetic retrieval of aerosol properties algorithm (SRAP) [59,60]. Finally, high spatial resolution AOD data of the Beijing area with 100 m spatial resolution are obtained [52]. The AOD data used in this study are those calculated in our previous study, and the validated correlation coefficient is approximately 0.88 in Beijing, which shows promising relationships [52].

2.4. Meteorological Data

Boundary layer height (BLH) data were provided through the ERA-5 from the European Centre for Medium-Range Weather Forecasts (http://www.ecmwf.int/, accessed on 4 December 2023). The meteorological data used in this study were provided in the database at a spatial resolution of 0.25° × 0.25°. The temporal resolution has various options, and to correspond to the hourly sampling frequency of $PM_{2.5/10}$, the temporal resolution of the products selected in this study was hourly. To correspond to the sampling times for $PM_{2.5}$ and PM_{10}, BLH values were obtained at 10:00 and 14:00 from the previous day.

Relative humidity (RH) data were obtained from the China regional multi-source fusion live analysis at 1 km resolution product (ART_1 km, ground). The 1 km-resolution product of China's regional multi-source fusion real-time analysis was developed by using ground station observations, satellites, numerical models, and other data, and includes four elements, such as hourly 2 m humidity. The product was provided by the China National Meteorological Operational Intranet (http://data.cma.cn/weatherGis/web/weather/weatherFcst/index, accessed on 4 December 2023).

2.5. Land-Use Variables

$PM_{2.5/10}$ concentrations are influenced by the subsurface of the land. Land-use data for Beijing in 2020 were collected from the Resource and Environment Data Cloud Platform (http://www.resdc.cn/, accessed on 4 December 2023). The data have a temporal resolution of years and are raster data with a spatial resolution of 1 km generated based on the 2015 land-use remote sensing monitoring data with Landsat TM imagery. The data include 6 primary types of land use (arable land, forest land, residential land, unused land, grassland, water) and 25 secondary types. The legend codes and their corresponding land-use types are listed in Table 1. Compared to China, Beijing lacks three land-use types: permanent glaciers and snow, Gobi, and others.

2.6. Simulation Data Fields

AOD and $PM_{2.5/10}$ simulation data were obtained from the CAMS (ECMWF Atmospheric Composition Reanalysis 4) global reanalysis (https://ads.atmosphere.copernicus.eu/, accessed on 7 December 2023). The $PM_{2.5}$, PM_{10}, and AOD data used in the present study have a horizontal resolution of 0.75° × 0.75° at 3 h temporal resolutions. Data were collected at 00:00, 03:00, 06:00, 09:00, 12:00, 15:00, 18:00, and 21:00 local time and then the 10:00 and 14:00 values were obtained by linear interpolation to make them correspond to the sampling times for $PM_{2.5}$ and PM_{10}. To begin with, the interval in which the unknown points are located was determined based on the eight known data points. Afterward, the weights were calculated using the distance between the unknown and known points. Assuming there is a linear relationship between the data points, the linear model was established based on the known values and the obtained weights. Two unknown moments as independent variables were substituted into the above linear model to calculate the estimations of the required moments.

2.7. Data Integration

In the present study, parameters from different categories were data integrated to ensure the spatial consistency of the data before being incorporated into the model. Meteorological data were resampled to 100 m spatial resolution using bilinear interpolation to obtain the same spatial and temporal resolution as AOD. Simultaneously, the land-use data were reprojected and resampled, and then stored as raster data in tiff format so that they had the same projection and spatial resolution as the AOD data. Furthermore, the AOD and PM data from CAMS were interpolated to have the same temporal resolution as the GF-1 AOD, allowing them to be used as input data in the proportional relationship formula method. Because the data in the large grid center was sampled as point data, the spatial interpolation was not performed on the CAMS data. Thereafter, the geographic location of the PM concentrations calculated by the proportional relationship formula method was assumed to be the center of each raster cell and then entered as supplemental site data. Finally, a grid with a spatial resolution of 100 m based on the AOD grid was created to integrate all PM data into records for the model.

3. Methods

The workflow of the present study is shown in Figure 2. Firstly, a proportional relationship formula was built to establish the refined $PM_{2.5/10}$ observation network combined with $PM_{2.5/10}$ measurements (Figure 3). Secondly, an IGTWR model that considers the main parameters, including the AOD, RH, and BLH, was developed to estimate ground $PM_{2.5}$ and PM_{10} concentrations [61]. The general distance was defined by latitude, longitude, and land-use classification data. The GTWR model had an encouraging performance with uniform and densely distributed input site observation data [62]. In the developed model, the site-measured PM data were replaced by the refined PM observation network. Finally, cross-validation and ground station validation were used to validate the model performance.

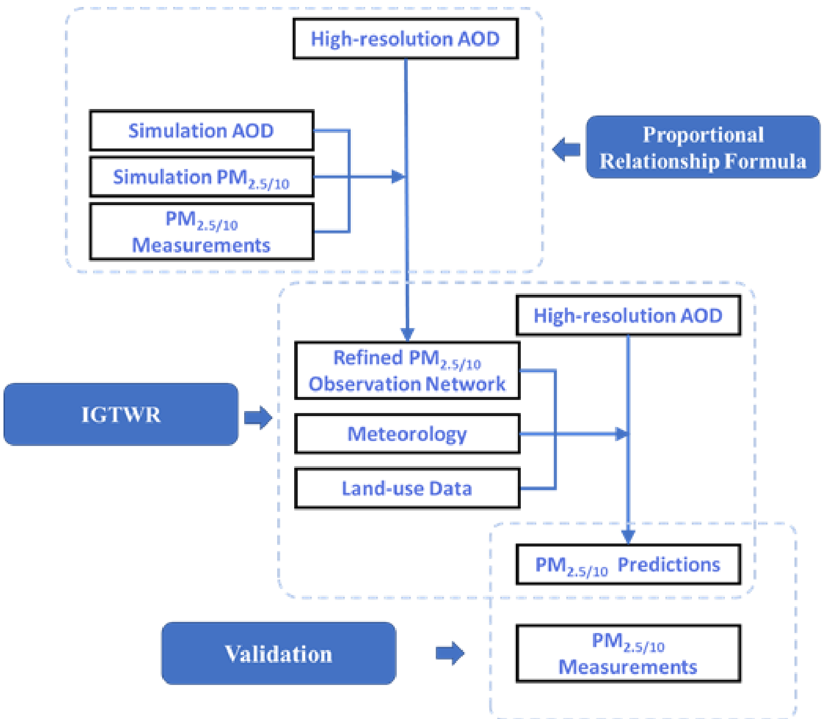

Figure 2. The workflow of proportional relationship formula (top box), improved geographically and temporally weighted regression (IGTWR) model (middle box), and model validation (bottom box).

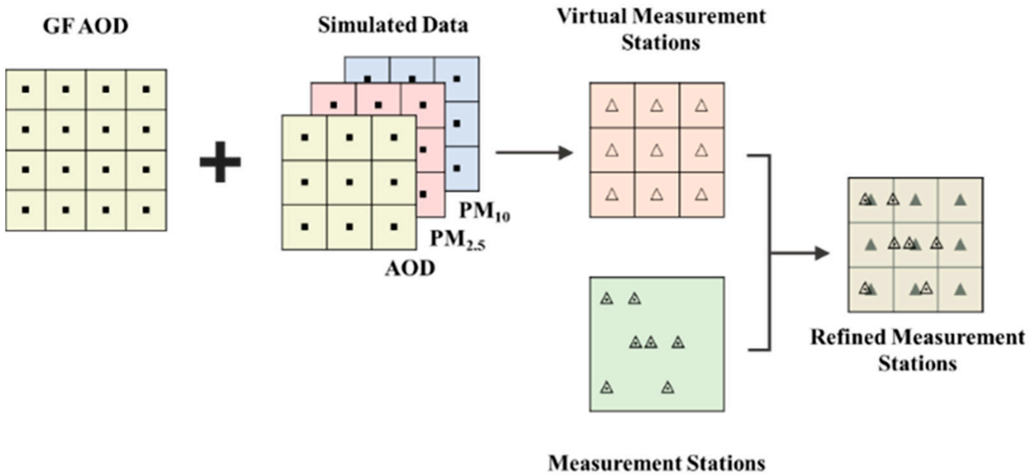

Figure 3. Flow chart for refined $PM_{2.5/10}$ monitoring stations using proportional relationship formula and other data.

3.1. Proportional Relationship Formula

Due to the vertical distribution and propagation properties possessed by AOD, a method for estimating $PM_{2.5}$ based on chemical transport models with AOD was proposed. The scaling factor was obtained from the AOD obtained from satellite remote sensing and the model-simulated AOD, and the actual $PM_{2.5}$ mass concentration was calculated using the scaling factor and the simulated $PM_{2.5}$ mass concentration [63]. In the present study, the scaling relationship equation was constructed as follows:

$$\begin{aligned} &\text{GF PRF PM}_{2.5/10}\text{ Concentration} \\ &= \frac{\text{Simulated Surface Level PM}_{2.5/10}\text{ Concentration}}{\text{Simulated Column AOD}} \times \text{GF AOD} \end{aligned} \quad (1)$$

The $PM_{2.5}$ or PM_{10} concentrations derived from this simple model were referred to as GF PRF $PM_{2.5/10}$ concentrations in the present study. The terms of particle mass concentrations employed in this analysis are summarized in Table 2.

Table 2. Definitions of terms used in this analysis.

Term	Unit	Definition
Simulated $PM_{2.5}$ concentration	mg/m^3	$PM_{2.5}$ or PM_{10} provided by CAMS, verification results with the 12 monitoring stations of the Ministry of Environmental Protection (MEP) within Beijing in 2020 show that the average R values are 0.59 and 0.43, respectively (https://cams2-82.aeroval.met.no/, accessed on 27 January 2024).
Simulated AOD	unitless	AOD provided by CAMS, verification results with the AeronetL1.5-d of Beijing station in 2020 show that the R and R^2 values are 0.80 and 0.89, respectively (https://cams2-82.aeroval.met.no/, accessed on 27 January 2024).
GF AOD	unitless	The TERRA and AQUA satellite MODIS data were first downscaled by GF-1 WFV data, then calculated the AOD by the SRAP algorithm.
GF PRF $PM_{2.5/10}$ concentration	μg/m^3	$PM_{2.5}$ or PM_{10} concentrations at 10:00 or 14:00 local time.

The study area was divided into a standard raster based on simulated AOD data resolution. The centroid position of each raster is used as the latitude and longitude of the fictitious station, and the simulation data are assigned to it.

3.2. IGTWR

Geographic data are affected not only by geographic location but also by time. Given this, a geographically time-weighted regression model was proposed [64]. Xue et al. [61] improved the GTWR model by redefining the generalized distance using land-use data, and the model obtained better performance. In the present study, the IGTWR model was used to estimate the mass concentrations of $PM_{2.5}$ and PM_{10} in the study area. The model is shown in (2):

$$y_i = \beta_0(u_0, v_0, d_0, h_0, l_0) + \sum_{k=1}^{d} \beta_k(u_0, v_0, d_0, h_0, l_0)x_{ik} + \varepsilon_i, i = 1, 2, \ldots, n \quad (2)$$

where u_0 and v_0 denote the longitude and latitude data, d_0 and h_0 denote the day and hour data, l_0 denotes land-use data, and d represents the number of independent variables. In this model, the independent variables are AOD, relative humidity, and boundary layer height; therefore, d is equal to 3 in this equation. i denotes the count of observation points in the refined observation network; y_i represents the estimated $PM_{2.5}$ or PM_{10} mass concentration. The EVI (enhanced vegetation index) can reflect the extent of capturing particulate matter on plant leaves [65], and NDVI can also be considered in the IGTWR model [66]. Because the study was conducted during the summer months, EVI and NDVI were not considered in the final model. The same fixed bandwidth is used in the present study.

4. Results and Validation

4.1. Results of the Model Fitting and Validation

A virtual monitoring network was established based on the proportional relationship formula in Beijing. $PM_{2.5}$ and PM_{10} were estimated using the refined $PM_{2.5/10}$ measurement network with GF AOD data.

Table 3 shows the coefficient (R^2), RMSE, and the coverage of the results for the different methods. The hybrid method of IGTWR and the chemical transport model-based proportional relationship formula was called GWC in this paper. A 1-year dataset was available for modeling in Beijing to obtain as much coverage as possible. In Beijing, $PM_{2.5/10}$ is positively proportional to AOD, due to $PM_{2.5/10}$ playing a major role in atmospheric extinction [67]. Higher planetary boundary layer height (PBLH) expands the near-surface atmosphere and promotes vertical convection [68], which means PBLH has a negative correlation with $PM_{2.5/10}$ mass concentration. As the $PM_{2.5/10}$ concentration measurement represents dry particles [21], higher air humidity leads to an increase in the value of AOD for the same $PM_{2.5/10}$ value [24]. Drying the sampling air stream at ground stations eliminates the influence of moisture on particulate mass concentrations when measuring particulate concentrations. Since it is obvious that atmospheric humidity also has a considerable impact on airborne contaminants, relative humidity is also included in the model's independent variables. That is, RH has a negative correlation with ground-level $PM_{2.5/10}$.

Table 3. Model performance using refined and unrefined site networks modeled separately, and coverage of results by different methods.

Method	R^2/RMSE	Coverage
$PM_{2.5}$ GWC	0.778/34.702 μg/m^3	92.91%
$PM_{2.5}$ GWR	0.660/25.434 μg/m^3	40.73%
PM_{10} GWC	0.741/49.757 μg/m^3	92.95%
PM_{10} GWR	0.550/38.052 μg/m^3	40.93%

A linear regression is performed to fit the $PM_{2.5/10}$ estimation to the monitored $PM_{2.5/10}$ concentration. Table 3 shows the R^2 and coverage of the improved and original models in this paper. These results indicated that $PM_{2.5/10}$ estimated by the hybrid model combined with GF AOD is in good agreement with $PM_{2.5}$ measurements on the ground. Moreover, with the inclusion of the "virtual site" data, the GWC model allows for the calculation of $PM_{2.5/10}$ concentrations using AOD data that do not cover the ground monitoring stations. Therefore, the hybrid model significantly improves the coverage of valid results.

4.2. PM Estimation Using Satellite Remotely Sensed Data

Figure 4 shows the seasonal $PM_{2.5/10}$ concentrations at a 100 m resolution. Figure 5 shows the annual mean $PM_{2.5/10}$ concentrations estimated by the IGTWR model at a 100 m resolution in 2020, respectively. Figure 6 shows $PM_{2.5/10}$ concentrations estimated by the IGTWR model at a resolution of 100 m for days with light pollution, heavy pollution, and pollution with prominent spatial characteristics. The polluted weather of $PM_{2.5}$ and PM_{10} in Beijing is mainly concentrated in winter, while spring and summer are mostly clean. In contrast, the distribution of PM values in the central and eastern urban areas is relatively stable, and the seasonal characteristics are relatively insignificant. Estimates of $PM_{2.5/10}$ in the eastern fringe were missing due to insufficient matching of the GF data. The results show that the spatial variation in the mass concentration of $PM_{2.5}$ is weaker in Beijing during the study time of this study, while the spatial variation in the mass concentration of PM_{10} is stronger. Particulate matter pollution is more severe in the urban and southeastern suburbs of southern Beijing, where the land has lower vegetation cover and higher population cover. The south-central part of the Beijing region is urban land, and this small area has lower and more stable $PM_{2.5}$ and PM_{10} concentrations compared to its neighboring regions. Relatively lighter pollution is found in the mountainous areas of northern and western Beijing, where estimated PM_{10} concentrations are typically below 40 μg/m^3. Highly polluted areas correspond to areas with poor vegetation cover and large populations. Conversely, clean areas are routinely characterized by thick vegetation, poor populations, and high altitudes. As industrial emissions and population density gradually increase from northwest to southeast in Beijing, PM_{10} also rises along the geographical gradient.

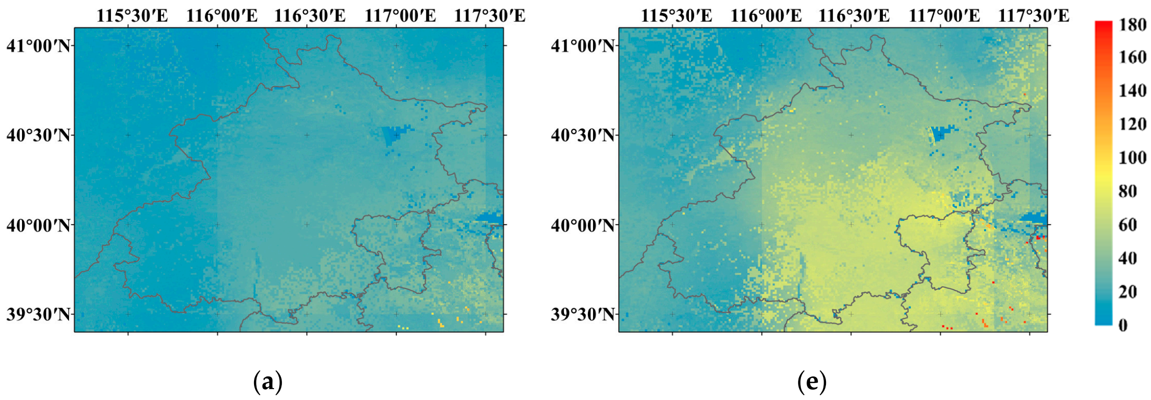

Figure 4. *Cont.*

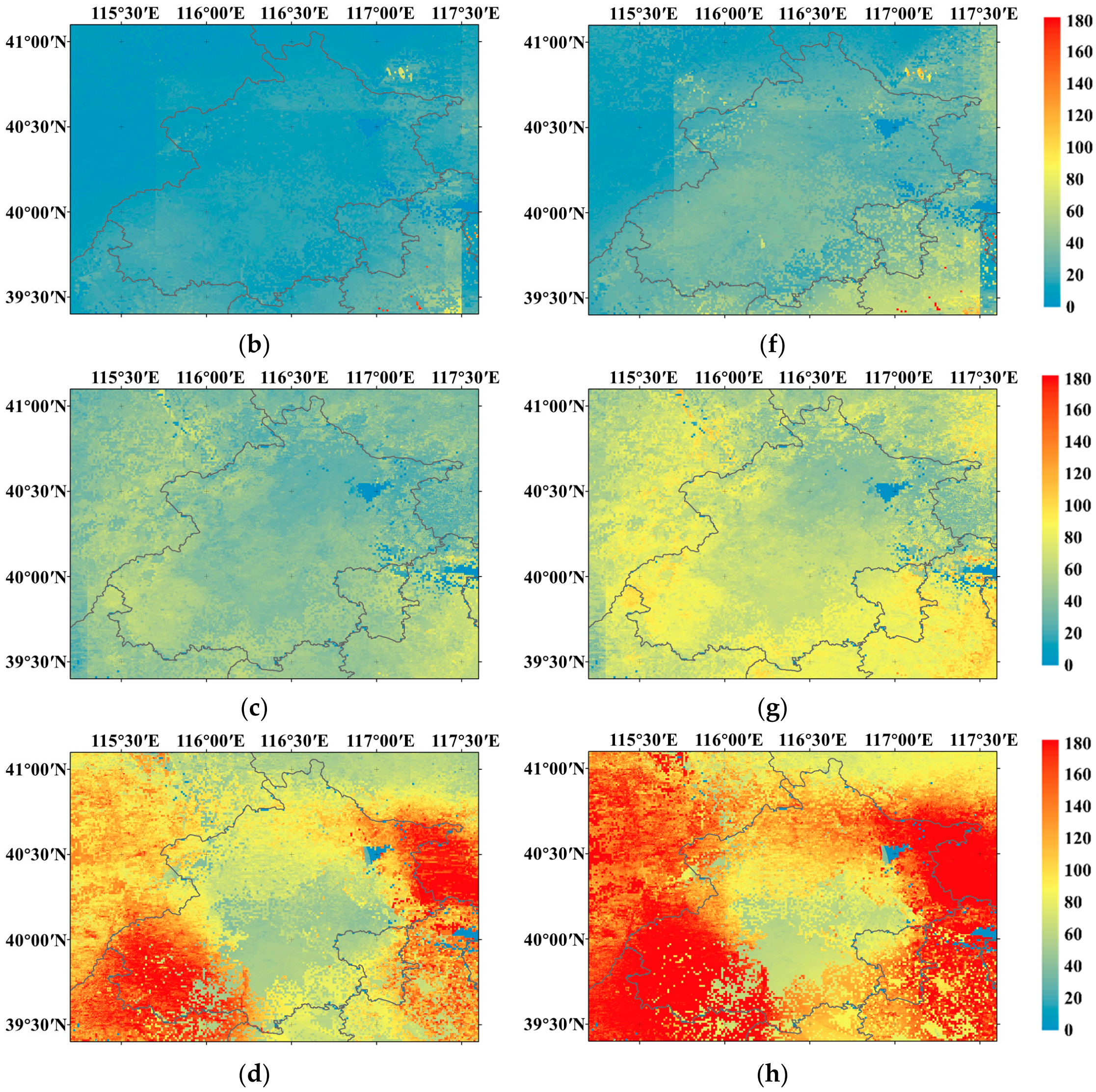

Figure 4. The distribution levels of seasonal mean $PM_{2.5}$ mass concentrations at 100 m resolution estimated by the model are shown for spring/summer/autumn/winter, (**a**), (**b**), (**c**), and (**d**), respectively. The monthly mean PM_{10} mass concentration distribution levels for spring/summer/autumn/winter are shown at 100 m resolution for the model estimates, (**e**), (**f**), (**g**), and (**h**), respectively. Estimates of $PM_{2.5/10}$ are missing at the eastern margin component due to insufficient matching of GF data.

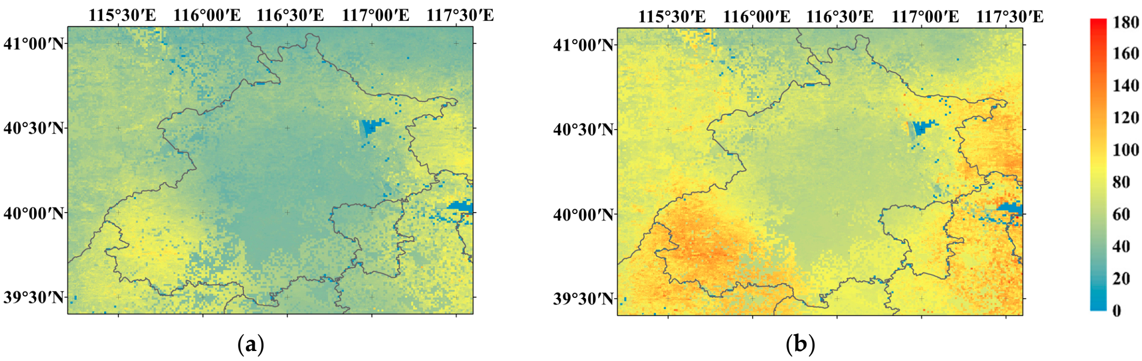

Figure 5. Model-estimated distribution levels of annual $PM_{2.5}$ (**a**) and PM_{10} (**b**) mass concentrations at 100 m resolution. Estimates of $PM_{2.5/10}$ are missing in the eastern margin component due to insufficient matching of GF data.

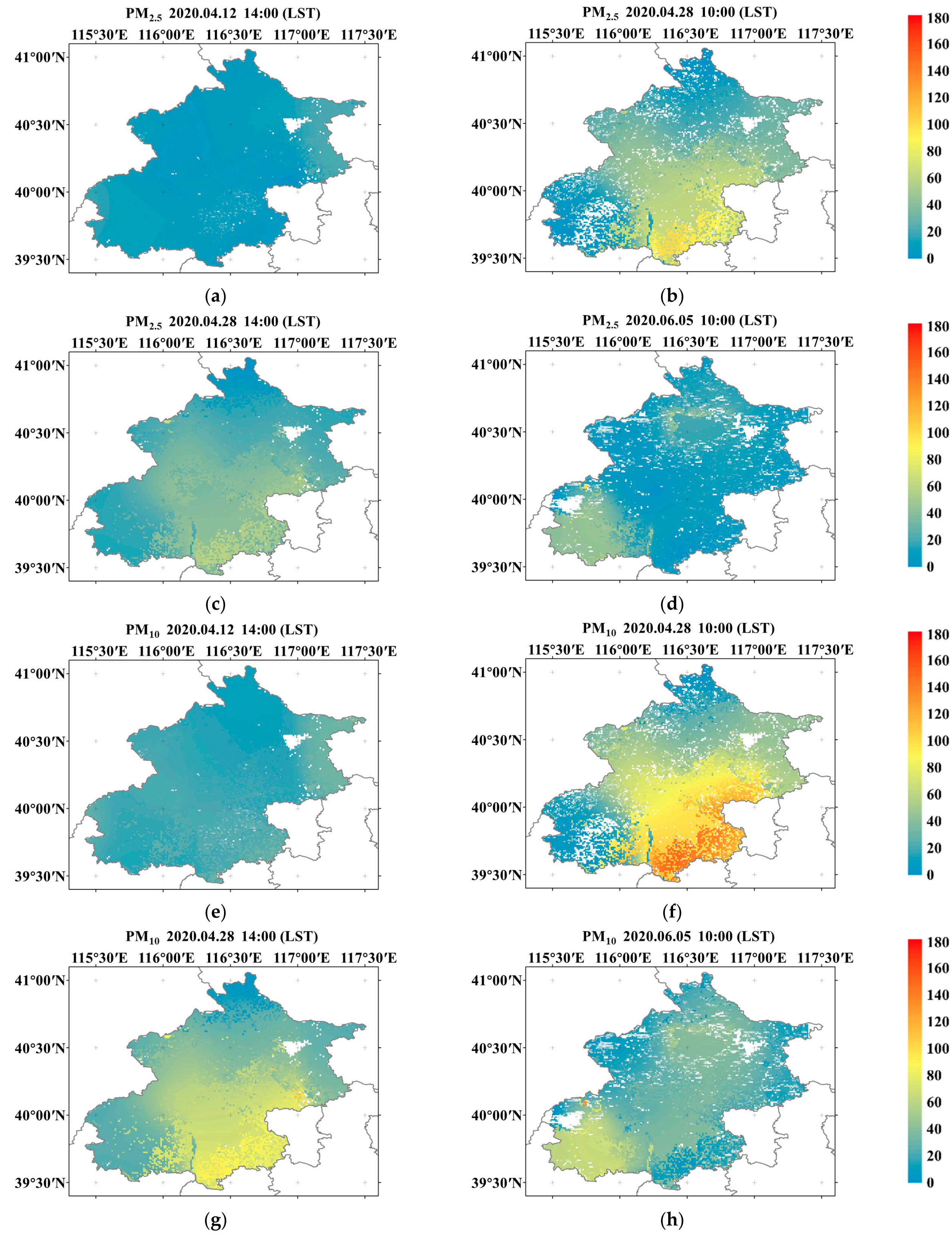

Figure 6. Distribution of $PM_{2.5}$ and PM_{10} mass concentrations (μm/m^3) at hourly resolution for clear and high pollution dates. The first row is $PM_{2.5}$ and the second row is PM_{10}, from left to right. Each column has the same time parameter, 14:00 on 12 April 2020 (**a**,**e**), 10:00 on 28 April 2020 (**b**,**f**), 14:00 on 28 April 2020 (**c**,**g**), and 10:00 on 5 June 2020 (**d**,**h**). The times are local standard time.

In addition, pollution in the study area is also influenced by pollutants from outside the region. For example, the southern suburbs are affected by pollution from polluted Hebei Province, south of Beijing [69]. In addition, previous studies have shown that the spatial characteristics of particulate matter in the Beijing area are similar to this study [51,69,70]. However, most of the $PM_{2.5/10}$ estimations are lower than the observations. This is primarily attributable to the fact that most air quality monitoring stations are located in the center of cities or counties with high pollution levels, while most data in remote mountainous areas are reflected in the estimation results with sparse pollution [69]. In addition, in the study area with large water coverage (such as Miyun Reservoir located northeast of Beijing), the calculated results of $PM_{2.5}$ and PM_{10} concentration levels are missing or low, which is the reason for the sudden change in data.

5. Discussion

5.1. Effects of the Refined $PM_{2.5/10}$ Measurement Stations

Three experiments were conducted to compare the performance impact of the measurement network before and after refining the model. The first way is to use the proportional relationship formula to refine the monitoring network and then use the IGTWR model to estimate $PM_{2.5/10}$. The second method of using the site data for IGTWR was called GWR in this paper. The third way is to use the proportional relationship formula method to obtain the PM concentration data as the virtual monitoring network to estimate $PM_{2.5/10}$. It was referred to as the PRF method. All three methods use the same bandwidth when calculating with the IGTWR model. Figures 7 and 8 show the validation results using the first two methods. Since there is no ground site as a training set, Figure 9 only shows the results obtained using the PRF method with the validation of the ground site (R^2 = 0.829, RMSE = 48.58 μg/m^3 and R^2 = 0.818, RMSE = 69.04 μg/m^3).

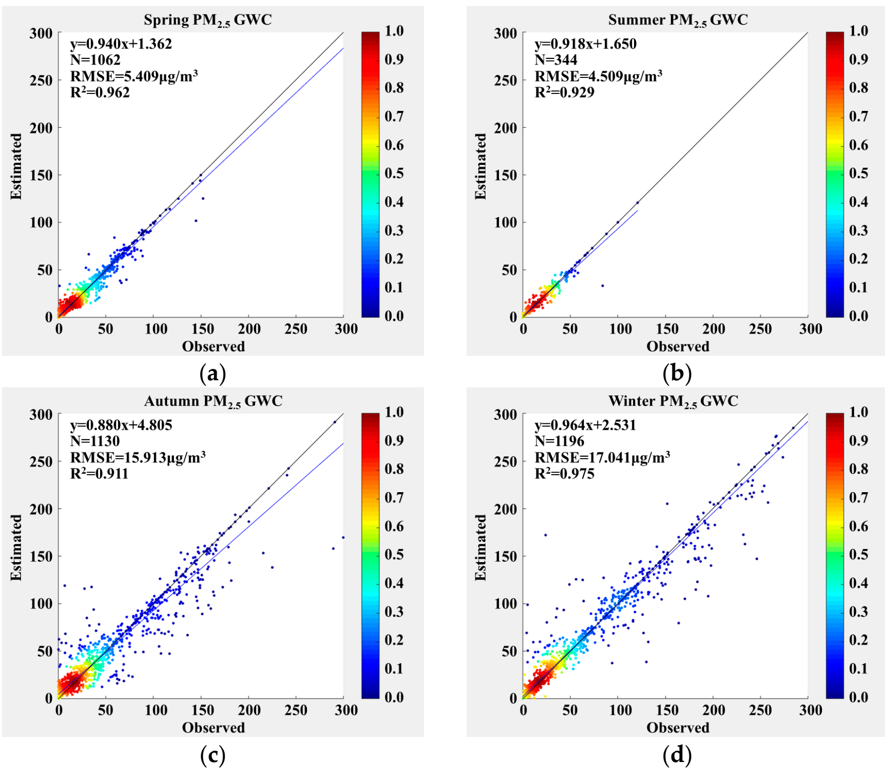

Figure 7. *Cont.*

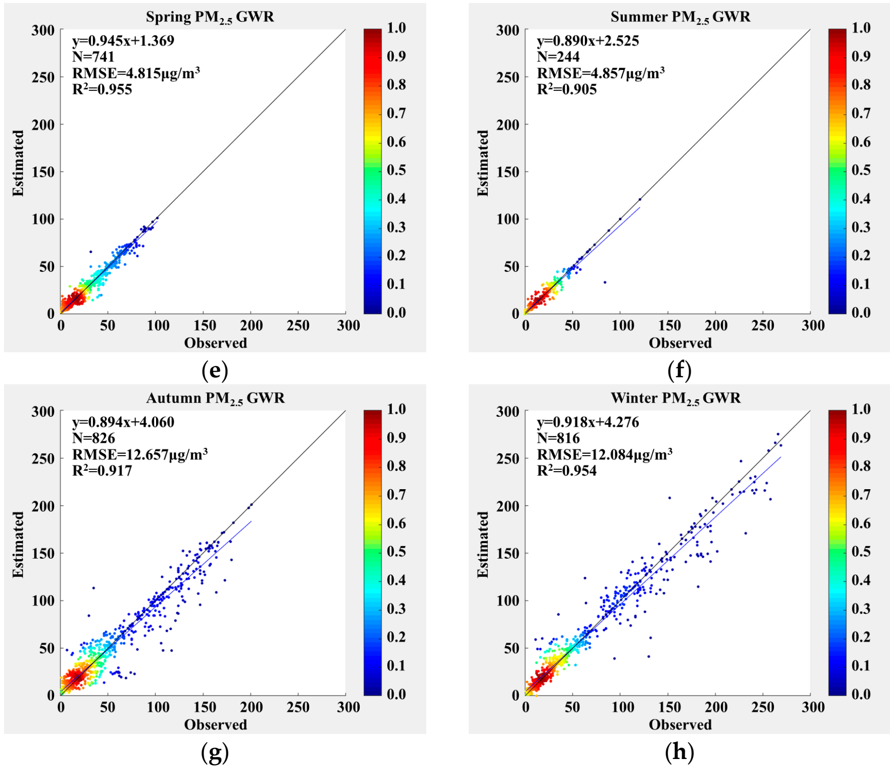

Figure 7. Cross-validation results for spring (**a**) summer (**b**) autumn (**c**) winter (**d**) based on the GWC model for $PM_{2.5}$. Cross-validation results for spring (**e**) summer (**f**) autumn (**g**) winter (**h**) based on the GWR model for $PM_{2.5}$. The solid black line is the 1:1 reference line.

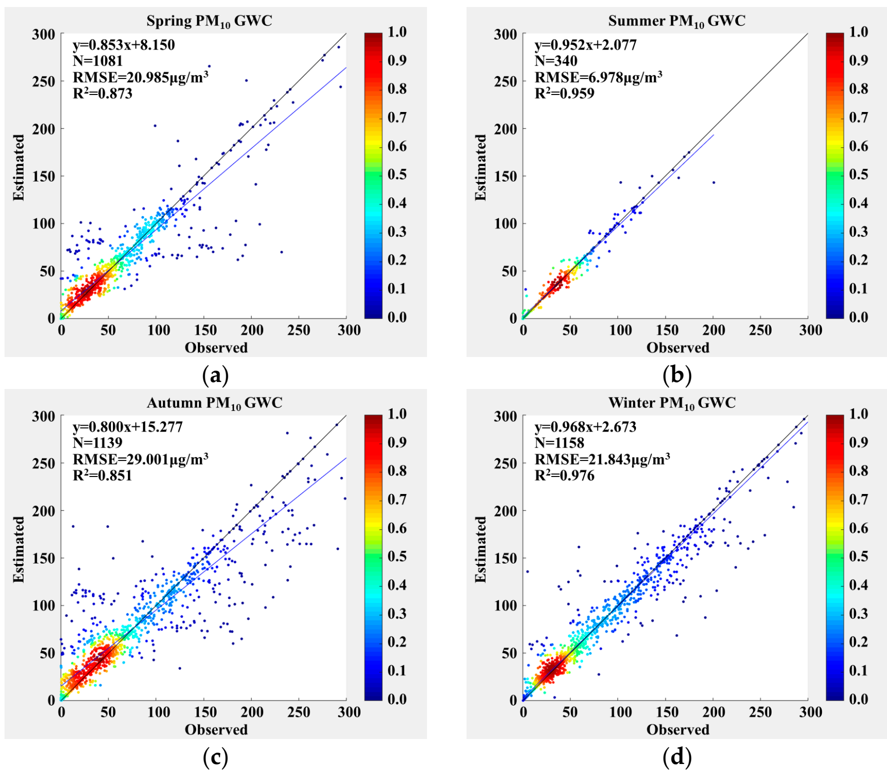

Figure 8. *Cont.*

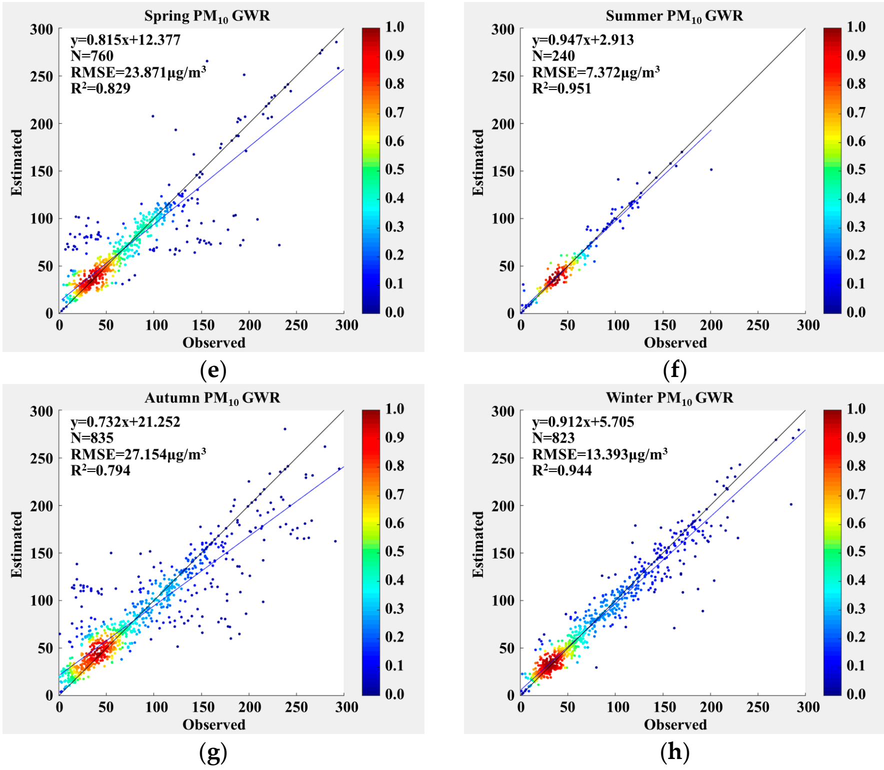

Figure 8. Cross-validation results for spring (**a**), summer (**b**), autumn (**c**), and winter (**d**) based on the GWC model for PM_{10}. Cross-validation results for spring (**e**), summer (**f**), autumn (**g**), and winter (**h**) based on the GWR model for PM_{10}.The solid black line is the 1:1 reference line.

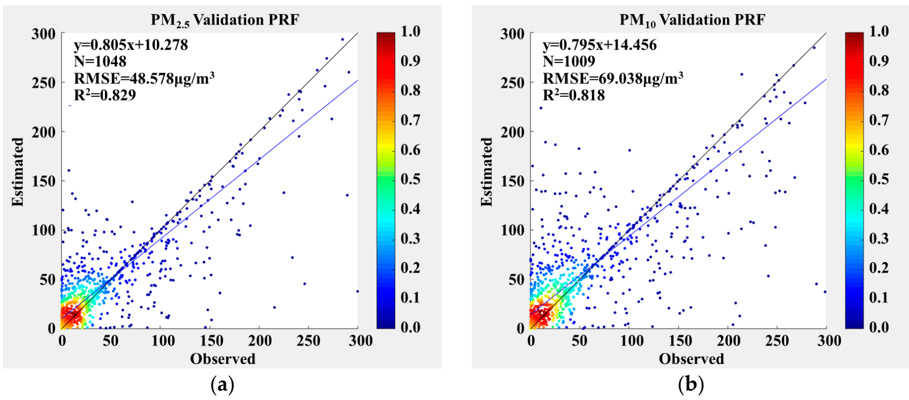

Figure 9. Validation of $PM_{2.5}$ mass concentrations calculated using the RPF against ground stations (**a**). Validation of PM_{10} mass concentrations calculated using the RPF against ground stations (**b**). The solid black line is the 1:1 reference line.

One of the characteristics of the GWR model is the need for uniform stations [62]. When the generalized distance is defined by both time and space, a uniform distribution of site data in time and space leads to better model results. The comparison of coverage is due to the uneven distribution of stations for the same bandwidth parameters, resulting in different coverage before and after the refined monitoring network. In areas far from the measurement sites, valid calculations could not be derived. The improved method in this study effectively improves the coverage calculated by the model without significantly reducing its effectiveness. The improved method in this study improved the 50% coverage.

The model performance was poor without ground stations, which means site data are indispensable in model calculations. However, the various verification results of GWR and GWC are similar, so refining the PM monitoring network by the virtual monitoring network will not cause much negative impact on the model fitting. In summary, the new model method can effectively improve the model performance under the optimal bandwidth.

The model estimated $PM_{2.5}$ with small seasonal differences, with R^2 above 0.9 in all cases. The model estimated PM_{10} with relatively large seasonal differences, mainly reflected in the R^2 below 0.9 in spring and fall, but the R^2 in winter was 0.97.

After refining the observation stations, the IGTWR model was tested for its ability to estimate $PM_{2.5/10}$ mass concentrations. Directly measured $PM_{2.5/10}$ data from the air quality monitoring sites within the study area (Figure 1) were used to perform validation analyses with the corresponding estimates. Regarding model fitting, the R^2 value of both $PM_{2.5}$ and PM_{10} models reached 0.94. The results showed that the IGTWR model performs well in hourly $PM_{2.5/10}$ estimation.

5.2. Comparisons with Other Studies

In previous studies, the cross-validation (CV) R^2 values for satellite-based ground-based $PM_{2.5/10}$ estimates ranged from 0.36 to 0.82 [16,71–75]. Among these studies, the hourly $PM_{2.5}$ estimates model (CV R^2 = 0.80) was found to perform significantly better than the daily $PM_{2.5}$ estimates model (CV R^2 = 0.61) due to its higher temporal matching characteristics.

In the present study, terrestrial sites were encrypted using the proportional relationship formula, thereby expanding the level of data coverage. In previous studies, average daily AOD associated with daily $PM_{2.5}$ and a seasonal linear regression model were used to estimate missing AOD and expand the level of data coverage [69]. Data discontinuities have a detrimental effect on model accuracy levels [69].

Figure 10 illustrates the monthly $PM_{2.5}$ mass concentration in this study compared to the monthly $PM_{2.5}$ mass concentration at 0.01° resolution published by Aaron van Donkelaar et al. [76]. The spatial distribution of $PM_{2.5}$ is characterized similarly in both datasets, proving the reliability of the PM distribution in this study.

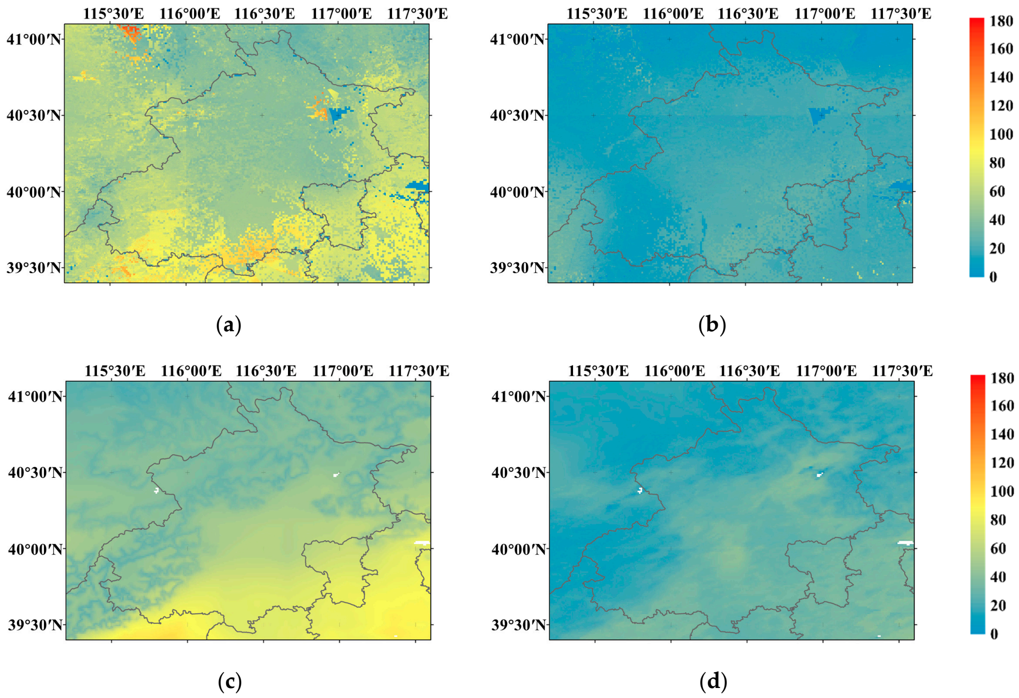

Figure 10. Distribution of monthly $PM_{2.5}$ mass concentrations at 100 m resolution (**a**,**b**) compared to the monthly $PM_{2.5}$ product (**c**,**d**) published by Aaron van Donkelaar et al. [76]. The left column is for January and the right is for April.

6. Conclusions

In this study, a virtual monitoring network for $PM_{2.5/10}$ was established by a proportional relationship formula. The IGTWR model and refined measurement network were applied to AOD. Then a hybrid model was proposed, which was applied to AOD, meteorological data, time and space data, and land-use data to estimate $PM_{2.5/10}$ mass concentrations in the study area at a spatial resolution of 100 m. The model results showed a reasonable spatial pattern similar to previous studies, with high values of $PM_{2.5/10}$ occurring mainly in urban and southeastern suburbs, and lower values in the northern and western mountainous regions in Beijing. The estimation result of $PM_{2.5}$ was validated by the ground stations with R^2 ranging from 0.91 to 0.98 and the RMSE ranging from 4.51 $\mu g/m^3$ to 17.04 $\mu g/m^3$, and that for PM_{10} was validated by the ground stations with R^2 ranging from 0.85 to 0.98 and the RMSE ranging from 6.98 $\mu g/m^3$ to 29.00 $\mu g/m^3$. This demonstrates the usability of the new hybrid model in the absence of sufficient AOD-monitoring data counterparts and provides a basis for future urban-scale PM estimates.

Despite these reliable results, some aspects of the model in this study could be improved. Firstly, the results of the model are influenced by the accuracy of the input AOD data, while the coverage of the results is also related to the AOD coverage. AOD data and meteorological field data with higher accuracy and resolution would benefit our model performance. Secondly, the temporal resolution of $PM_{2.5/10}$ data affects the model performance [69]. Therefore, more time continuity in the AOD data was needed to improve model performance. Finally, as the association between ground-level $PM_{2.5/10}$ and AOD is influenced by many different factors, more variables will be considered in our future studies (such as population density, road length, and emission information).

Author Contributions: Conceptualization, S.W., Y.S. and R.B.; methodology, S.W. and Y.S.; validation, S.W., Y.S. and R.B.; formal analysis, S.W.; investigation, Y.S.; resources, S.W., Y.S., R.B. and C.J.; data curation, S.W. and Y.S.; writing—original draft preparation, S.W. and Y.S.; writing—review and editing, Y.X. and Y.S.; visualization, Y.S.; supervision, Y.X. and X.J.; funding acquisition, Y.X. All authors have read and agreed to the published version of the manuscript.

Funding: This work was supported in part by the National Natural Science Foundation of China (NSFC) under Grant No. 42275147.

Data Availability Statement: Data are contained within the article.

Acknowledgments: The authors thank all data providers for their efforts in making the data available: the $PM_{2.5/10}$ ground-based measurement data from the Chinese National Real-Time Air Quality Release Platform; BLH data from the European Centre for Medium-Range Weather Forecasts; RH data from the China National Meteorological Operational Intranet; land-use data from the Resource and Environment Data Cloud Platform; and AOD and $PM_{2.5/10}$ simulation data from the CAMS (ECMWF Atmospheric Composition Reanalysis 4) global reanalysis.

Conflicts of Interest: The authors declare no conflict of interest.

References

1. Beelen, R.; Raaschou-Nielsen, O.; Stafoggia, M.; Andersen, Z.J.; Weinmayr, G.; Hoffmann, B.; Wolf, K.; Samoli, E.; Fischer, P.; Nieuwenhuijsen, M.; et al. Effects of long-term exposure to air pollution on natural-cause mortality: An analysis of 22 European cohorts within the multicentre ESCAPE project. *Lancet* **2014**, *383*, 785–795. [CrossRef] [PubMed]
2. Crouse, D.L.; Peters, P.A.; van Donkelaar, A.; Goldberg, M.S.; Villeneuve, P.J.; Brion, O.; Khan, S.; Atari, D.O.; Jerrett, M.; Pope, C.A.; et al. Risk of Non accidental and Cardiovascular Mortality in Relation to Long-term Exposure to Low Concentrations of Fine Particulate Matter: A Canadian National-Level Cohort Study. *Environ. Health Perspect.* **2012**, *120*, 708–714. [CrossRef] [PubMed]
3. Dimitrova, R.; Lurponglukana, N.; Fernando, H.J.S.; Runger, G.C.; Hyde, P.; Hedquist, B.C.; Anderson, J.; Bannister, W.; Johnson, W. Relationship between particulate matter and childhood asthma – basis of a future warning system for central Phoenix. *Atmos. Chem. Phys.* **2012**, *12*, 2479–2490.
4. Hoek, G.; Krishnan, R.M.; Beelen, R.; Peters, A.; Ostro, B.; Brunekreef, B.; Kaufman, J.D. Long-term air pollution exposure and cardio- respiratory mortality: A review. *Environ. Health* **2013**, *12*, 43. [CrossRef] [PubMed]
5. Pascal, M.; Falq, G.; Wagner, V.; Chatignoux, E.; Corso, M.; Blanchard, M.; Host, S.; Pascal, L.; Larrieu, S. Short-term impacts of particulate matter (PM_{10}, $PM_{10–2.5}$, $PM_{2.5}$) on mortality in nine French cities. *Atmos. Environ.* **2014**, *95*, 175–184. [CrossRef]

6. Ballester, F.; Estarlich, M.; Iniguez, C.; Llop, S.; Ramon, R.; Esplugues, A.; Lacasana, M.; Rebagliato, M. Air pollution exposure during pregnancy and reduced birth size: A prospective birth cohort study in Valencia, Spain. *Environ. Health* **2010**, *9*, 6. [CrossRef] [PubMed]
7. Lim, S.S.; Vos, T.; Flaxman, A.D.; Danaei, G.; Shibuya, K.; Adair-Rohani, H.; AlMazroa, M.A.; Amann, M.; Anderson, H.R.; Andrews, K.G.; et al. A comparative risk assessment of burden of disease and injury attributable to 67 risk factors and risk factor clusters in 21 regions, 1990–2010: A systematic analysis for the Global Burden of Disease Study 2010. *Lancet* **2012**, *380*, 2224–2260. [CrossRef] [PubMed]
8. Rohde, R.A.; Muller, R.A. Air Pollution in China: Mapping of Concentrations and Sources. *PLoS ONE* **2015**, *10*, e0135749. [CrossRef]
9. Geng, G.; Zhang, Q.; Martin, R.V.; van Donkelaar, A.; Huo, H.; Che, H.; Lin, J.; He, K. Estimating long-term $PM_{2.5}$ concentrations in China using satellite-based aerosol optical depth and a chemical transport model. *Remote Sens. Environ.* **2015**, *166*, 262–270. [CrossRef]
10. Peng, J.; Chen, S.; Lu, H.; Liu, Y.; Wu, J. Spatiotemporal patterns of remotely sensed $PM_{2.5}$ concentration in China from 1999 to 2011. *Remote Sens. Environ.* **2016**, *174*, 109–121. [CrossRef]
11. Hu, J.; Wang, Y.; Ying, Q.; Zhang, H. Spatial and temporal variability of $PM_{2.5}$ and PM_{10} over the North China Plain and the Yangtze River Delta, China. *Atmos. Environ.* **2014**, *95*, 598–609. [CrossRef]
12. Hu, X.; Waller, L.A.; Lyapustin, A.; Wang, Y.; Al-Hamdan, M.Z.; Crosson, W.L.; Estes, M.G.; Estes, S.M.; Quattrochi, D.A.; Puttaswamy, S.J.; et al. Estimating ground-level $PM_{2.5}$ concentrations in the Southeastern United States using MAIAC AOD retrievals and a two-stage model. *Remote Sens. Environ.* **2014**, *140*, 220–232. [CrossRef]
13. Qian, Z.; He, Q.; Lin, H.M.; Kong, L.; Bentley, C.M.; Liu, W.; Zhou, D. High Temperatures Enhanced Acute Mortality Effects of Ambient Particle Pollution in the "Oven" City of Wuhan, China. *Environ. Health Perspect.* **2008**, *116*, 1172–1178. [CrossRef]
14. Hu, X.; Waller, L.A.; Lyapustin, A.; Wang, Y.; Liu, Y. 10-year spatial and temporal trends of $PM_{2.5}$ concentrations in the southeastern US estimated using high-resolution satellite data. *Atmos. Chem. Phys.* **2014**, *14*, 6301–6314. [CrossRef]
15. Lee, M.C.; Huang, N. Changes in self-perceived economic satisfaction and mortality at old ages: Evidence from a survey of middle-aged and elderly adults in Taiwan. *Soc. Sci. Med.* **2015**, *130*, 1–8. [CrossRef] [PubMed]
16. Ma, Z.; Hu, X.; Huang, L.; Bi, J.; Liu, Y. Estimating Ground-Level $PM_{2.5}$ in China Using Satellite Remote Sensing. *Environ. Sci. Technol.* **2014**, *48*, 7436–7444. [CrossRef]
17. Zou, B.; Pu, Q.; Bilal, M.; Weng, Q.; Zhai, L.; Nichol, J.E. High-Resolution Satellite Mapping of Fine Particulates Based on Geographically Weighted Regression. *IEEE Geosci. Remote Sens. Lett.* **2016**, *13*, 495–499. [CrossRef]
18. Engel-Cox, J.A.; Holloman, C.H.; Coutant, B.W.; Hoff, R.M. Qualitative and quantitative evaluation of MODIS satellite sensor data for regional and urban scale air quality. *Atmos. Environ.* **2004**, *38*, 2495–2509. [CrossRef]
19. Schaap, M.; Apituley, A.; Timmermans, R.M.A.; Koelemeijer, R.B.A.; de Leeuw, G. Exploring the relation between aerosol optical depth and $PM_{2.5}$ at Cabauw, the Netherlands. *Atmos. Chem. Phys.* **2009**, *9*, 909–925. [CrossRef]
20. Hutchison, K.D.; Smith, S.; Faruqui, S.J. Correlating MODIS aerosol optical thickness data with ground-based $PM_{2.5}$ observations across Texas for use in a real-time air quality prediction system. *Atmos. Environ.* **2005**, *39*, 7190–7203. [CrossRef]
21. Liu, Y.; Sarnat, J.A.; Kilaru, V.; Jacob, D.J.; Koutrakis, P. Estimating Ground-Level $PM_{2.5}$ in the Eastern United States Using Satellite Remote Sensing. *Environ. Sci. Technol.* **2005**, *39*, 3269–3278. [CrossRef]
22. Kim, G.; Lee, S.; Im, J.; Song, C.K.; Kim, J.; Lee, M. Aerosol data assimilation and forecast using Geostationary Ocean Color Imager aerosol optical depth and in-situ observations during the KORUS-AQ observing period. *Giscience Remote Sens.* **2021**, *58*, 1175–1194. [CrossRef]
23. Li, Y.; Xue, Y.; Guang, J.; She, L.; Fan, C.; Chen, G. Ground-Level $PM_{2.5}$ Concentration Estimation from Satellite Data in the Beijing Area Using a Specific Particle Swarm Extinction Mass Conversion Algorithm. *Remote Sens.* **2018**, *10*, 1906. [CrossRef]
24. Lin, C.; Li, Y.; Yuan, Z.; Lau, A.K.H.; Li, C.; Fung, J.C.H. Using satellite remote sensing data to estimate the high-resolution distribution of ground-level $PM_{2.5}$. *Remote Sens. Environ.* **2015**, *156*, 117–128. [CrossRef]
25. van Donkelaar, A.; Martin, R.V.; Brauer, M.; Boys, B.L. Use of Satellite Observations for Long-Term Exposure Assessment of Global Concentrations of Fine Particulate Matter. *Environ. Health Perspect.* **2015**, *123*, 135–143. [CrossRef] [PubMed]
26. Zhang, X.; Chu, Y.; Wang, Y.; Zhang, K. Predicting daily $PM_{2.5}$ concentrations in Texas using high-resolution satellite aerosol optical depth. *Sci. Total Environ.* **2018**, *631–632*, 904–911. [CrossRef]
27. Gupta, P.; Christopher, S.A. Seven year particulate matter air quality assessment from surface and satellite measurements. *Atmos. Chem. Phys.* **2008**, *8*, 3311–3324. [CrossRef]
28. Kloog, I.; Nordio, F.; Coull, B.A.; Schwartz, J. Incorporating Local Land Use Regression and Satellite Aerosol Optical Depth In A Hybrid Model Of Spatiotemporal $PM_{2.5}$ Exposures In The Mid-Atlantic States. *Environ. Sci. Technol.* **2012**, *46*, 11913–11921. [CrossRef] [PubMed]
29. Unnithan, S.L.K.; Gnanappazham, L. Spatiotemporal mixed effects modeling for the estimation of $PM_{2.5}$ from MODIS AOD over the Indian subcontinent. *Giscience Remote Sens.* **2020**, *57*, 159–173. [CrossRef]
30. He, Q.; Zhang, M.; Song, Y.; Huang, B. Spatiotemporal assessment of $PM_{2.5}$ concentrations and exposure in China from 2013 to 2017 using satellite-derived data. *J. Clean. Prod.* **2021**, *286*, 124965. [CrossRef]
31. Li, S.X.; Zou, B.; Fang, X.; Lin, Y. Time series modeling of $PM_{2.5}$ concentrations with residual variance constraint in eastern mainland China during 2013–2017. *Sci. Total Environ.* **2020**, *710*, 135755. [CrossRef]

32. Xue, W.H.; Zhang, J.; Zhong, C.; Ji, D.Y.; Huang, W. Satellite-derived spatiotemporal $PM_{2.5}$ concentrations and variations from 2006 to 2017 in China. *Sci. Total Environ.* **2020**, *712*, 134577. [CrossRef]
33. You, W.; Zang, Z.; Zhang, L.; Li, Y.; Wang, W. Estimating national-scale ground-level PM25 concentration in China using geographically weighted regression based on MODIS and MISR AOD. *Environ. Sci. Pollut. Res.* **2016**, *23*, 8327–8338. [CrossRef]
34. Chen, G.; Knibbs, L.D.; Zhang, W.; Li, S.; Cao, W.; Guo, J.; Ren, H.; Wang, B.; Wang, H.; Williams, G.; et al. Estimating spatiotemporal distribution of PM1 concentrations in China with satellite remote sensing, meteorology, and land use information. *Environ. Pollut.* **2018**, *233*, 1086–1094. [CrossRef] [PubMed]
35. Hua, Z.; Sun, W.; Yang, G.; Du, Q. A Full-Coverage Daily Average $PM_{2.5}$ Retrieval Method with Two-Stage IVW Fused MODIS C6 AOD and Two-Stage GAM Model. *Remote Sens.* **2019**, *11*, 1558. [CrossRef]
36. She, Q.; Choi, M.; Belle, J.H.; Xiao, Q.; Bi, J.; Huang, K.; Meng, X.; Geng, G.; Kim, J.; He, K.; et al. Satellite-based estimation of hourly $PM_{2.5}$ levels during heavy winter pollution episodes in the Yangtze River Delta, China. *Chemosphere* **2020**, *239*, 124678. [CrossRef]
37. Stafoggia, M.; Bellander, T.; Bucci, S.; Davoli, M.; de Hoogh, K.; de'Donato, F.; Gariazzo, C.; Lyapustin, A.; Michelozzi, P.; Renzi, M.; et al. Estimation of daily PM_{10} and $PM_{2.5}$ concentrations in Italy, 2013–2015, using a spatiotemporal land-use random-forest model. *Environ. Int.* **2019**, *124*, 170–179. [CrossRef]
38. Chen, W. Estimating $PM_{2.5}$ with high-resolution 1-km AOD data and an improved machine learning model over Shenzhen, China. *Sci. Total Environ.* **2020**, *746*, 141093. [CrossRef] [PubMed]
39. Guo, B.; Zhang, D.; Pei, L.; Su, Y.; Wang, X.; Bian, Y.; Zhang, D.; Yao, W.; Zhou, Z.; Guo, L. Estimating $PM_{2.5}$ concentrations via random forest method using satellite, auxiliary, and ground-level station dataset at multiple temporal scales across China in 2017. *Sci. Total Environ.* **2021**, *778*, 146288. [CrossRef]
40. Wei, J.; Li, Z.; Xue, W.; Sun, L.; Fan, T.; Liu, L.; Su, T.; Cribb, M. The ChinaHighPM_{10} dataset: Generation, validation, and spatiotemporal variations from 2015 to 2019 across China. *Environ. Int.* **2021**, *146*, 106290. [CrossRef] [PubMed]
41. Jung, C.R.; Hwang, B.F.; Chen, W.T. Incorporating long-term satellite-based aerosol optical depth, localized land use data, and meteorological variables to estimate ground-level $PM_{2.5}$ concentrations in Taiwan from 2005 to 2015. *Environ. Pollut.* **2018**, *237*, 1000–1010. [CrossRef]
42. Xu, Y.; Ho, H.C.; Wong, M.S.; Deng, C.; Shi, Y.; Chan, T.C.; Knudby, A. Evaluation of machine learning techniques with multiple remote sensing datasets in estimating monthly concentrations of ground-level $PM_{2.5}$. *Environ. Pollut.* **2018**, *242*, 1417–1426. [CrossRef]
43. Chen, B.; You, S.; Ye, Y.; Fu, Y.; Ye, Z.; Deng, J.; Wang, K.; Hong, Y. An interpretable self-adaptive deep neural network for estimating daily spatially-continuous $PM_{2.5}$ concentrations across China. *Sci. Total Environ.* **2021**, *768*, 144724. [CrossRef] [PubMed]
44. Li, T.; Shen, H.; Zeng, C.; Yuan, Q.; Zhang, L. Point-surface fusion of station measurements and satellite observations for mapping $PM_{2.5}$ distribution in China: Methods and assessment. *Atmos. Environ.* **2017**, *152*, 477–489. [CrossRef]
45. Zang, L.; Mao, F.; Guo, J.; Wang, W.; Pan, Z.; Shen, H.; Zhu, B.; Wang, Z. Estimation of spatiotemporal PM1.0 distributions in China by combining $PM_{2.5}$ observations with satellite aerosol optical depth. *Sci. Total Environ.* **2019**, *658*, 1256–1264. [CrossRef]
46. Song, W.; Jia, H.; Huang, J.; Zhang, Y. A satellite-based geographically weighted regression model for regional $PM_{2.5}$ estimation over the Pearl River Delta region in China. *Remote Sens. Environ.* **2014**, *154*, 1–7. [CrossRef]
47. He, Q.; Huang, B. Satellite-based high-resolution $PM_{2.5}$ estimation over the Beijing-Tianjin-Hebei region of China using an improved geographically and temporally weighted regression model. *Environ. Pollut.* **2018**, *236*, 1027–1037. [CrossRef] [PubMed]
48. Liu, K.; Wu, Y.; Wang, X.; Wang, C. Impact of the spatial structure of urban agglomerations on air pollution in China. *China Popul.·Resour. Environ.* **2020**, *30*, 28–35.
49. Huo, F.; Xu, L.; Li, Y.; Famiglietti, J.S.; Li, Z.; Kajikawa, Y.; Chen, F. Using big data analytics to synthesize research domains and identify emerging fields in urban climatology. *Wiley Interdiscip. Rev. Clim. Chang.* **2021**, *12*, e688. [CrossRef]
50. Sun, K.; Chen, X.; Zhu, Z.; Zhang, T. High Resolution Aerosol Optical Depth Retrieval Using Gaofen-1 WFV Camera Data. *Remote Sens.* **2017**, *9*, 89. [CrossRef]
51. Zhang, T.; Zhu, Z.; Gong, W.; Zhu, Z.; Sun, K.; Wang, L.; Huang, Y.; Mao, F.; Shen, H.; Li, Z.; et al. Estimation of ultrahigh resolution $PM_{2.5}$ concentrations in urban areas using 160 m Gaofen-1 AOD retrievals. *Remote Sens. Environ.* **2018**, *216*, 91–104. [CrossRef]
52. Bai, R.; Xue, Y.; Jiang, X.; Jin, C.; Sun, Y. Retrieval of High-Resolution Aerosol Optical Depth for Urban Air Pollution Monitoring. *Atmosphere* **2022**, *13*, 756. [CrossRef]
53. Han, L.; Zhou, W.; Li, W.; Li, L. Impact of urbanization level on urban air quality: A case of fine particles ($PM_{2.5}$) in Chinese cities. *Environ. Pollut.* **2014**, *194*, 163–170. [CrossRef] [PubMed]
54. Van Donkelaar, A.; Martin, R.V.; Brauer, M.; Kahn, R.; Levy, R.; Verduzco, C.; Villeneuve, P.J. Global Estimates of Ambient Fine Particulate Matter Concentrations from Satellite-Based Aerosol Optical Depth: Development and Application. *Environ. Health Perspect.* **2010**, *118*, 847–855. [CrossRef]
55. Xu, X.; Liu, J.; Zhuang, D. Remote sensing Monitoring methods of land use/cover changes in national scale. *Anhui Agric. Sci.* **2012**, *40*, 2365–2369.
56. Li, Z.; Shen, H.; Li, H.; Xia, G.; Gamba, P.; Zhang, L. Multi-feature combined cloud and cloud shadow detection in GaoFen-1 wide field of view imagery. *Remote Sens. Environ.* **2017**, *191*, 342–358. [CrossRef]

57. Johnson, K.; Cole-Rhodes, A.; Zavorin, I.; Le Moigne, J. Mutual information as a similarity measure for remote sensing image registration. *Geo-Spat. Image Data Exploit. II* **2001**, *4383*, 51–61.
58. Li, Y.; Xue, Y.; He, X.; Guang, J. High-resolution aerosol remote sensing retrieval over urban areas by synergetic use of HJ-1 CCD and MODIS data. *Atmos. Environ.* **2012**, *46*, 173–180. [CrossRef]
59. Xue, Y.; He, X.W.; Xu, H.; Guang, J.; Guo, J.P.; Mei, L.L. China Collection 2.0: The aerosol optical depth dataset from the synergetic retrieval of aerosol properties algorithm. *Atmos. Environ.* **2014**, *95*, 45–58. [CrossRef]
60. Xue, Y.; Cracknell, A.P. Operational bi-angle approach to retrieve the Earth surface albedo from AVHRR data in the visible band. *Remote Sens.* **1995**, *16*, 417–429. [CrossRef]
61. Xue, Y.; Li, Y.; Guang, J.; Tugui, A.; She, L.; Qin, K.; Fan, C.; Che, Y.; Xie, Y.; Wen, Y.; et al. Hourly $PM_{2.5}$ Estimation over Central and Eastern China Based on Himawari-8 Data. *Remote Sens.* **2020**, *12*, 855. [CrossRef]
62. Shin, M.; Kang, Y.; Park, S.; Im, J.; Yoo, C.; Quackenbush, L.J. Estimating ground-level particulate matter concentrations using satellite-based data: A review. *Giscience Remote Sens.* **2020**, *57*, 174–189. [CrossRef]
63. Liu, Y.; Park, R.J.; Jacob, D.J.; Li, Q.B.; Kilaru, V.; Sarnat, J.A. Mapping annual mean ground-level $PM_{2.5}$ concentrations using Multiangle Imaging Spectroradiometer aerosol optical thickness over the contiguous United States. *J. Geophys. Res.-Atmos.* **2004**, *109*, 10. [CrossRef]
64. Huang, B.; Wu, B.; Barry, M. Geographically and temporally weighted regression for modeling spatio-temporal variation in house prices. *Int. J. Geogr. Inf. Sci.* **2010**, *24*, 383–401. [CrossRef]
65. Pugh, T.A.M.; MacKenzie, A.R.; Whyatt, J.D.; Hewitt, C.N. Effectiveness of Green Infrastructure for Improvement of Air Quality in Urban Street Canyons. *Environ. Sci. Technol.* **2012**, *46*, 7692–7699. [CrossRef] [PubMed]
66. Sun, Y.; Xue, Y.; Jiang, X.; Jin, C.; Wu, S.; Zhou, X. Estimation of the $PM_{2.5}$ and PM_{10} Mass Concentration over Land from FY-4A Aerosol Optical Depth Data. *Remote Sens.* **2021**, *13*, 4276. [CrossRef]
67. Wu, J.; Yao, F.; Li, W.; Si, M. VIIRS-based remote sensing estimation of ground-level $PM_{2.5}$ concentrations in Beijing–Tianjin–Hebei: A spatiotemporal statistical model. *Remote Sens. Environ.* **2016**, *184*, 316–328. [CrossRef]
68. Miao, Y.; Liu, S.; Guo, J.; Huang, S.; Yan, Y.; Lou, M. Unraveling the relationships between boundary layer height and $PM_{2.5}$ pollution in China based on four-year radiosonde measurements. *Environ. Pollut.* **2018**, *243*, 1186–1195. [CrossRef]
69. Guo, Y.; Tang, Q.; Gong, D.Y.; Zhang, Z. Estimating ground-level $PM_{2.5}$ concentrations in Beijing using a satellite-based geographically and temporally weighted regression model. *Remote Sens. Environ.* **2017**, *198*, 140–149. [CrossRef]
70. Zhang, Y.; Li, Z. Remote sensing of atmospheric fine particulate matter ($PM_{2.5}$) mass concentration near the ground from satellite observation. *Remote Sens. Environ.* **2015**, *160*, 252–262. [CrossRef]
71. Guo, Y.; Feng, N.; Christopher, S.A.; Kang, P.; Zhan, F.B.; Hong, S. Satellite remote sensing of fine particulate matter ($PM_{2.5}$) air quality over Beijing using MODIS. *Int. J. Remote Sens.* **2014**, *35*, 6522–6544. [CrossRef]
72. Li, R.; Gong, J.; Chen, L.; Wang, Z. Estimating Ground-Level $PM_{2.5}$ Using Fine-Resolution Satellite Data in the Megacity of Beijing, China. *Aerosol Air Qual. Res.* **2015**, *15*, 1347–1356. [CrossRef]
73. Liu, Y.; Servant, A.; Guy, O.J.; Al-Jamal, K.T.; Williams, P.R.; Hawkins, K.M.; Kostarelos, K. An electric-field responsive microsystem for controllable miniaturised drug delivery applications. *Sens. Actuators B Chem.* **2012**, *175*, 100–105. [CrossRef]
74. Xie, Y.; Wang, Y.; Zhang, K.; Dong, W.; Lv, B.; Bai, Y. Daily Estimation of Ground-Level $PM_{2.5}$ Concentrations over Beijing Using 3 km Resolution MODIS AOD. *Environ. Sci. Technol.* **2015**, *49*, 12280–12288. [CrossRef]
75. Xin, J.; Zhang, Q.; Wang, L.; Gong, C.; Wang, Y.; Liu, Z.; Gao, W. The empirical relationship between the $PM_{2.5}$ concentration and aerosol optical depth over the background of North China from 2009 to 2011. *Atmos. Res.* **2014**, *138*, 179–188. [CrossRef]
76. van Donkelaar, A.; Hammer, M.S.; Bindle, L.; Brauer, M.; Brook, J.R.; Garay, M.J.; Hsu, N.C.; Kalashnikova, O.V.; Kahn, R.A.; Lee, C.; et al. Monthly Global Estimates of Fine Particulate Matter and Their Uncertainty. *Environ. Sci. Technol.* **2021**, *55*, 15287–15300. [CrossRef]